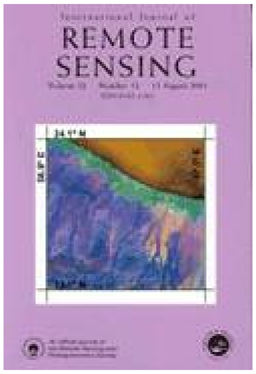

Integrating remote sensing into forest ecosystem modeling through Bayesian calibration

Journal:	*International Journal of Remote Sensing*
Manuscript ID:	TRES-SIP-2006-0033
Manuscript Type:	Special Issue Paper
Date Submitted by the Author:	09-Oct-2006
Complete List of Authors:	Patenaude, Genevieve; University of Edinburgh, School of Geosciences Milne, Ronald; Centre for Ecology and Hydrology, Edinburgh Van Oijen, Marcel; Centre for Ecology and Hydrology, Edinburgh Rowland, Clare; Centre for Ecology and Hydrology, Section for Earth Observation Hill, Ross; Centre for Ecology and Hydrology, Section for Earth Observation
Keywords:	FORESTRY, HYPERSPECTRAL DATA, LIDAR, SAR
Keywords (user defined):	Bayesian, Uncertainty, Ecological modelling

Abstract

Process-based models have been used to simulate 3 dimensional complexities of forest ecosystems and their temporal changes but their extensive data requirement and complex parameterisation has often limited their use for practical management applications. Increasingly, information retrieved with remote sensing techniques can help in model parameterisation and data collection by providing spatially and temporally resolved forest information. In this paper, we illustrate the potential of Bayesian calibration for integrating such data sources to simulate forest production. As an example, we use the 3-PG model combined with hyperspectral, LiDAR, SAR and field-based data to simulate the growth of UK Corsican pine stands. Hyperspectral, LiDAR and SAR data are used to estimate LAI dynamics, tree height and above ground biomass respectively, while the Bayesian calibration provides estimates of uncertainties to model parameters and outputs. The Bayesian calibration contrasts with goodness-of-fit approaches which do not provide uncertainties to parameters and model outputs. Parameters and the data used in the calibration process are presented in the form of probability distributions, reflecting our degree of certainty about them. After the calibration, the distributions are updated. To approximate posterior distributions (of outputs and parameters), a Markov Chain Monte Carlo sampling approach is used (25000 steps). A sensitivity analysis is also conducted between parameters and outputs. Overall, the results illustrate the potential of a Bayesian framework for truly integrative work, both in the consideration of field-based and remotely sensed datasets available and in estimating parameter and model output uncertainties.

1 Introduction

Process-based models are widely used in the fields of forest physiology and forest ecology as they enable deeper insights into the drivers of forest production and growth and offer higher flexibility than conventional production tables (Landsberg & Waring 1997). This flexibility enables the quantification and prediction of forest 2 and 3-D structural variables owing to deterministic, mechanistic and/or stochastic algorithms simulating the processes affecting growth. However, their practical value has often been limited owing to (a) their extensive data requirement and (b) their complexity and the difficulty in quantifying parameters and model output uncertainty (e.g. Gertner et al. 1999).

Remote sensing technology is increasingly exploited for forest inventorying and monitoring (e.g. Baulies and Pons 1995, Hyyppä et al. 2000) as it can provide insights into the spatial and temporal variability of forests, information which is seldom available from ground surveys alone. While it is a generally accepted premise that field data provide the closest representation of reality, spatially resolved ground based data can be time consuming, expensive and logistically difficult to acquire where access to forested land is limited. Comparatively, highly resolved remote sensing data can be obtained at relatively low costs. Additionally, novel approaches now supply estimates of forest structural variables of accuracy equivalent if not superior to traditional measurements techniques (e.g. Magnussen and Boudewyn 1998, Hyyppä *et al.* 2001). Remote sensing may therefore help meet forest ecophysiologists and modellers' data requirements.

In this context, we present Bayesian calibration (BC) as a means to integrate remotely acquired datasets into ecological models. This approach offers a number of advantages in comparison with goodness-of-fit and optimisation approaches. In addition to facilitating the integration of data of varying degree of uncertainty, BC enables the quantification of uncertainty associated with parameters and model outputs, an important requirement for practical applications of models (Green *et al.* 2000). Parameters and data used in the calibration process are presented in the form of probability distributions, reflecting our degree of certainty about them (Jansen 1999). Bayesian calibration enables the updating of distributions as further information is gained. The framework thereby targets the much-needed platform for (i) integrating datasets of varying degree of certainty and (ii) expressing parameter and output uncertainty in forest-growth modelling (Green et al. 2000, Ghazoul & McAllister 2003, Van Oijen et al. 2005).

In this paper, we demonstrate the usefulness of the approach by calibrating the 3-PG model (Physiological Processes Predicting Growth, Landsberg & Waring 1997, Sands & Landsberg 2002) for UK Corsican pine stands (*Pinus nigra* car. *maritima* (AIT.) Melv.). 3-PG is built on a combination of process-based calculations, several key simplifying assumptions and few empirical relationships. The model predicts gross and net primary production as well as biomass allocation to different pools. Over the years, it has been increasingly and successfully been applied to new species worldwide (Landsberg & Waring 1997, Law *et al.* 2000, Waring 2000, Coops & Waring 2001, Coops *et al.* 2001, Sands & Landsberg 2002, Almeida *et al.* 2004, Stape *et al.* 2004). However, the parameterisation of the model for new species remains a challenge. As stated by Sands (2004, p.3): “In only a few cases have parameters characterising a species been rigorously determined, and even then this has been largely by a process of trial and error”. In this context, the aim of this paper is to illustrate the potential of BC as a means to (i) calibrate models for novel species (ii) integrate multi-source datasets and (iii) quantify model parameters and outputs along with uncertainty.

Our paper is structured as follow. In section two, we present an overview of the 3-PG principal submodels. Section three provides a description of the field site, available remote sensing and field based datasets for model initialisation, parameterisation and calibration. The processing of the databases is also briefly summarised. Section four contains the description of the Bayesian calibration and finally, results and discussions are presented in section five and six, respectively.

2 Structure of the 3-PG model

The 3-PG model has monthly or annual time steps and entails five state variables – foliage, stem and root biomass, stocking density and available soil water – in conjunction with five submodels –biomass production; biomass allocation; soil water availability and evapotranspiration; mortality; and inventory variables. The required climatic data are monthly average values of solar radiation (MJ m^{-2} d^{-1}), atmospheric water pressure deficit (mbar), mean air temperature (°C), rainfall (mm $month^{-1}$) and frost days. Other input variables include site latitude, an estimate of soil fertility, maximum available soil water (mm per depth of rooting zone, in meters) and a general description of soil texture. 3-PG outputs considered in this study were leaf area index (LAI, projected), above ground biomass (ABG biomass, t ha^{-1}), stem biomass (t ha^{-1}), foliage biomass (t ha^{-1}), root biomass (t ha^{-1}) and stem height (m).

2.1 Biomass production

The biomass submodel converts solar radiation into dry matter. The interception of radiation is defined by Beer's law and canopy LAI. The amount of photosynthetically active radiation intercepted by a stand ($ø_{\mathrm{pa}}$, mol MJ^{-1}) is then converted into carbohydrates by means of a canopy quantum efficiency coefficient (α_{cx}, mol mol^{-1}) and a conversion factor converting carbohydrates into dry matter. Further constraints on assimilation are then applied by dimensionless environmental factors varying between 0 and 1 (1 indicates optimal conditions). These factors, also referred to as modifiers, are multiplicative and represent the influence of vapour pressure deficit (D) or soil moisture, which ever is most limiting, mean air temperature (T), frost, and soil nutrition on photosynthetic assimilation (Sands 2004). Gross primary productivity (P_g, t ha^{-1} d^{-1}) is then converted to net primary productivity (P_n, t ha^{-1} d^{-1}) using a simple P_n / P_g ratio (Y).

2.2 Biomass allocation and mortality

P_n is then allocated to the different plant components (roots, foliage and stems including branches) at each time step. Allocation to roots is proportional to the harshness of the environment. It is influenced by site fertility, stand age and the most limiting between D or soil water, but does not fall below or exceed set values of minimum and maximum allocation to roots. The remaining P_n is shared between stems and foliage through a foliage-to-stem allocation ratio, given by an allometric relationship with mean diameter at breast height (Sands & Landsberg 2002, Sands 2004). DBH is itself obtained from an allometric relationship with stem biomass. Whereas P_n partitioning parameters must generally be estimated from fitting methods, those pertaining to the allometric relationship between stem biomass and diameter can be derived from forest mensuration (Sands & Landsberg 2002). Mortality is applied through the self thinning 3/2 law, which sets an upper limit to the mean single-tree stem mass at a given stocking level.

2.3 Soil water balance

Available soil water θ (mm month^{-1}) is governed by rainfall interception by the canopy (i_R), rainfall (R_P, mm month^{-1}) and evapotranspiration (E_T, mm month^{-1}). If the maximum available water at saturation is exceeded, the excess of water is lost as runoff.

$$\theta = (1 - i_R)R_P - E_T \qquad [1]$$

Rainfall interception increases with canopy LAI and is taken as a fraction of rainfall. E_T is calculated using the Penman Monteith equation controlled by the canopy conductance, solar radiation and D. Canopy conductance (g_C, m s^{-1}) increases with LAI but is bounded by the LAI value at which conductance is at a maximum (g_{Cx}, m s^{-1}). The relationship between g_C and LAI is further controlled by age and the most limiting factor controlling stomatal aperture, either vapor pressure deficit or soil moisture. Further details on 3-PG can be found in Landsberg and Waring (1997) and Sands and Landsberg (2002).

3 Materials and methods

3.1 Study site and available datasets

The calibration of the 3-PG model was conducted for Corsican Pine stands of yield class 14 using existing data from a 20,000 ha forest plantation, East Anglia, UK (Thetford forest, 52°30′ N, 0°30′ E). The stands in Thetford are assumed under an intermediate spacing, intermediate thinning and 80 years rotation regime (Edwards & Christie 1981).

3.2 Field based datasets

The following datasets were used in the calibration: (i) the UK Forestry Commission GIS database, a spatially exhaustive catalogue comprising of approximate stand level information on species, yield class, planting year, planting density and stemwood volume (ii) the Maestro-1 1989 campaign and the 2000 SHAC campaign datasets (Baker 1992, Baker et al. 1994, Skinner and Luckman, 2000) which consist of ground data collected on stand level information (each sampled stand was allocated a Forestry Commission code maintaining consistency with the GIS database) and (iii) datasets collected in Thetford over the years (e.g. Ovington 1957, Corbett 1973, Roberts 1976, Beadle et al. 1982, Beadle et al. 1985a, Beadle et al. 1985b, Beadle et al. 1985c, Stewart 1988, Mencuccini & Grace 1996).

The model was initialised for a stand aged 15 years using chronosequenced biomass data obtained from the Maestro dataset (Baker 1992, Baker et al. 1994). Initialising the model at this age removes the need for extra parameterisation required by early growth processes while still enabling the calibration of key parameters. Root, stem and foliage biomass were 7.1 t/ha, 22 t/ha and 9.8 t/ha respectively. Initial stocking of 3955 trees per hectare was obtained from the production tables (Edwards and Christie 1981).

The required climatic data were derived from the Climate Research Unit datasets and the Cambridge botanical garden meteorological station (New et al. 2000, http://badc.nerc.ac.uk/home/index.html). The area is characterised by a relatively flat topography and insignificant climatic variations within the site were assumed (Ovington 1957). Long term average climatic conditions are summarized in Table 1.

Table 1

Other input variables include site latitude, an estimate of soil fertility and texture, as well as available soil water (mm per depth of rooting zone, in meters). The soils of the plantation are of poor quality, predominantly sandy with deep alkaline chalky bedrock and drain freely throughout the forest (Corbett 1973, Mencuccini & Grace 1996). Minimum available water was estimated based on field measurements taken during the drought year of 1976. During the drought, measurements have shown that at least 170mm soil water was available (Roberts et al. 1982). The maximum available water was assumed as 250mm based on: (a) the assumption that storage capacity for sandy soils is approximately 150mm per metre of soil with a permanent wilting point of 50 mm and (b) field measurements taken in Thetford, showing that 95% of roots are located in the first meter of soil (Roberts 1976). Given the documented deep bedrock (Corbett 1973), we assumed a 2 meters soil layer.

All runs were made with 3-PGpjs, a Visual Basic implementation of 3-PG in Excel available at http://www.ffp.csiro.au/fap/3pg/download_details.htm.

3.3. Remote sensing datasets and processing

SAR, Hyperspectral, and LiDAR datasets acquired in 2000 were included in the calibration. These datasets were used instead of alternative empirical, approximate yield based tables given their site specific nature and our ability to quantify variability in the estimates of biophysical variables.

3.3.1 SAR

A multi-frequency, Synthetic Aperture Radar instrument (E-SAR) was flown on the 31st May 2000 in wide swath mode, with data collected at L-HH, L-HV, L-VV, X-

VV, plus repeat-pass L-band fully polarimetric data. The mean stand backscatter coefficient, σ^0 (dB), and the mean stand interferometric coherence were calculated for the L-HH, L-VV and L-HV polarisations from the geocoded E-SAR data. Although InSAR data were available, only the interferometric coherence and backscatter were used for the work described here. A neural network was trained to estimate stand top height in Corsican Pine stands from the E-SAR backscatter and coherence data. The data were divided in half, with half used as a training data set to train the neural network and the other half used as a testing data set, to assess the ability of the proposed relationships against unseen data. The inputs to the network were the three mean stand values for coherence (L-HH, L-HV, L-VV) plus the three mean stand values for backscatter (L-HH, L-HV, L-VV). The neural network was a 1-hidden layer network trained with a Levenberg-Marquardt based learning algorithm. Two network structures were investigated, with 2 and 11 nodes in the hidden layer, respectively. To ensure that the best network was selected, 50 trained networks were generated, with the best network selected based on minimum RMSE against the test data set. The lowest error was produced by a network with two nodes in the hidden layer resulting in a R^2 of 0.90 and a RMSE of 2.51m when tested against the test data set (Rowland et al. 2003).

3.3.2 Hyperspectral

Hyperspectral data was acquired using the SHAC HyMAP imaging spectrometer in June 2000 (126 contiguous bands, 436-2486 nm at 15 nm spectral resolution, 4m spatial resolution). Atmospheric correction was applied by DLR and the overlapping scenes were georectified, mosaicked and normalised to minimise the effect of sensor look angle. Signal to noise ratio analysis was conducted to remove noisy atmospheric water absorption bands from the original dataset.

3.3.3 LiDAR

E-SAR and hyperspectral datasets were complemented in June 2000 with first and last return data acquired by means of a small footprint Airborne Laser Terrain Mapper (Optech ALTM 1210). The ALTM emits laser pulses at a wavelength of 1047nm (NIR) where vegetation is highly reflective. The data was collected at footprint size of 0.05m^2. A ±10º scanning orientation perpendicular to the flight path was selected which generated irregular ground measurements ranging between 2.80m^2 to 6.50m^2. The precision of the instrument was estimated at 0.60m in the x and y position and 0.15 m in z (www.optech.on.ca).

A digital canopy height model (DCHM) was obtained by subtraction of a digital terrain model (DTM) from a digital surface model (DSM). The DSM and the DTM were derived from the first and last significant LiDAR returns respectively (methodology described in Gaveau and Hill 2003, Patenaude et al. 2004 and Rowland et al. 2003). Both the first and last return were converted from a point to a gridded format. The DTM was then produced by applying a minimum value filter to identify local height minima in the gridded LiDAR last return product. Top height per stand was extracted from the DCHM based on the maximum canopy height per stand (R^2=0.94, RMSE 1.68m, bias 0.48m). The use of percentiles was also tested (90th, 95th, 97.5th and 99th). However, whilst they may be appropriate for mean stand height, they were found to underestimate canopy top height for the Thetford stands (Rowland et al. 2003).

4 Bayesian calibration

In Bayesian statistics, probability is interpreted as the degree of certainty for some quantity, conditional to available data and knowledge. As model parameter values are not precisely known, this uncertainty can be represented as a probability distribution over the parameters. Thus, if we define θ as a parameter vector for 3-PG, then P(θ) represents its probability distribution and P(f(θ)) the uncertainty in model outputs (f(θ)) generated by the uncertainty in the parameters. In this context, Bayesian calibration is a method enabling P(θ) to be updated as new data come in (e.g. Figure 1).

Figure 1

Given a dataset D, we can derive P(θ|D) from P(θ) by applying Bayes Theorem:

$$P(\theta|D) = P(\theta)\ P(D|\theta) / P(D) \qquad [2]$$

In Bayesian terminology and as illustrated in Figure 1, P(θ|D) is the updated or posterior parameter distribution; P(θ) is the original distribution, referred to as the prior; P(D|θ) is the conditional probability of the data for a given parameterisation, called the likelihood; and P(D) is a normalization constant that may be referred to as the evidence.

4.1 The prior

The prior distribution is built from marginal distributions, which reflect our current knowledge of parameters and outputs. The distribution that best describes the available information about parameters must be used. When limited information is available, Van Oijen *et al.* (2005) suggest the use of uniform distributions, bounded by a biophysically or biologically reasonable maximum and minimum value for each parameter. Table 2 presents values to 3-PG parameters and the prior distribution selected for calibration.

Table 2

The prior distributions were set uniform, bounded by a maximum and minimum value for each parameter. Boundaries to the prior were obtained from direct observation on Corsican pine stands in Thetford (CP-T), from literature on Corsican or other pine species (P-L), from surrogate species or 3-PG set default values (D) or finally as best guess estimates or fitting approaches (F) (Table 2). Key parameters difficult to measure in the field and for which little information was available were included in the calibration. The remaining parameters were prescribed constant values (Table 2), including the parameters pertaining to the allometric relationship between stem mass and diameter at breast height (a_S and n_S).

4.2 The likelihood

A total of 28 data points were used in the calibration exercise: LiDAR derived heights (4); E-SAR and field based estimates of total above-ground biomass (4 and 1 respectively); field based estimates of stem, foliage and root biomass (3, 3 and 5 respectively); and Hyperspectral and ground based LAI estimates (7 and 1 respectively).

4.2.1 LiDAR heights

LiDAR heights were taken as surrogates of top heights (section 3.3.3). These were aggregated and averaged per 15 years age classes (Figure 2). Uncertainty was estimated as standard deviations to height averages per class. An additional ±0.5 m error was added to small samples (n<9).

4.2.2 E-SAR and field based above-ground biomass

Above-ground biomass data were derived from E-SAR top height estimates. Conversion of top height to above ground biomass involved two stages of calculations (Rowland et al. 2003, summarised here): (i) conversion of top height to stemwood volume using an empirical relationship derived from Edwards & Christie (1981) (ii) conversion of stemwood volume to biomass using a biomass expansion factor and a generic basic density coefficient (1.5 for temperate pine species, Milne 1992, IPCC 2004; 0.43 t m^{-3}, Hamilton 1975, respectively). E-SAR biomass estimates were plotted against yield table estimates (log transformed, Figure 2). Untransformed standard deviations of biomass (aggregated and averaged per 15 years age classes) were used as error estimates. An additional ±10 t ha^{-1} uncertainty was added to small samples (n<9).

Figure 2

4.2.3 Stem, foliage and root biomass

Stem and foliage biomass data points were derived from Baker (1992) and Baker et al. (1994). For root biomass, a root to shoot ratio was derived from destructive measurements made in 6 mature Scot pine stands (Ovington, 1957). The ratio below to above-ground across ages (0.3, Std 0.05) was assumed representative to that of Corsican pine. This value is also consistent with that given by the IPCC (2003) for temperate coniferous forests. Five root biomass points were derived. A ±10% relative error was assumed.

4.2.4 LAI

Given the absence of ground based or alternative sources, LAI data points were derived from hyperspectral data. LAI in pine plantations generally exhibit a growth pattern expressed as (e.g. Mencuccini and Grace 1996):

$$LAI = ae^{-0.5\left(\frac{\ln(x/x_0)}{b}\right)^2} \qquad [3]$$

Where a represents the maximum LAI reached by a stand, x_0 the age at which this maximum is reached and b, a parameter controlling the tailing off of the LAI curve. Equation 3 was solved in a three way procedure: (i) Corsican pine stands in the GIS database were co-registered to the image allowing the chronosequencing of leaf area index (LAI) throughout the rotation (ii) based on the results by Lee et al. (2004) and Pu and Gong (2004) where close proportionality was found between LAI and the primary axis of a principal component analysis (PCA) for the different wavelengths, PCA was used to estimate LAI growth patterns in Thetford CP stands. Averaged values per stand were plotted against stand age using the GIS attribute database. The x_0 and *b* parameters, which pertain to the shape of the curve only, not the magnitude of LAI were solved by minimising the distance between chronological PCA points and the Equation 3 (Figure 3). (iii) Conversion of PCA values to LAI, was completed using the available projected LAI datum (Ovington, 1957). Large relative uncertainties (30%) were assumed.

Figure 3

4.2.4 Estimating the likelihood

To calculate the likelihood, i.e. the probability of the data given a model parameterisation P(D|θ), information about measurement error must be available. Assuming that the errors associated with our data are independent and Gaussian, P(D|θ) then follows from the comparison of each data point D_i with the corresponding model output $f_i(\theta)$ as:

$$P(D|\theta) = \prod_{i}^{n} \varphi(D_i - \mathrm{f}_i(\theta); 0, SD_i) \qquad [4]$$

where, φ symbolizes a Gaussian function with 0 and SD_i as mean and standard deviation of errors, and n=28, the number of points in the data sample.

4.3 The posterior: a Monte Carlo estimation of the posterior distribution

The application of Bayes Theorem to process-based models has traditionally been hampered by two problems: (i) the models cannot be solved analytically, so a sampling method to explore the parameter space is required (we define parameter space as the space entailing all combinations of possible parameter vectors defined by the prior) (ii) the models need to be run at every sampled point in parameter space (to calculate the probability), a highly time consuming and computer intensive process. In recent years, Markov Chain Monte Carlo (MCMC) methods have been found useful to resolve this type of problem (Van Oijen et al. 2005). Here, we used the MCMC Metropolis Hastings Random Walk, which has the two following steps:

1. After randomly choosing a first parameter vector, propose a new candidate for the next parameter vector in the chain from the parameter space as:

$$\theta' = \theta_t + \varepsilon \qquad [5]$$

Where θ' is the proposed candidate, θ_t is the current parameter vector and ε is a random vector enabling the exploration of the parameter space. ε is selected from a Gaussian distribution with mean 0. Its standard deviation should be chosen to enable a wide exploration of the parameter space and to yield acceptance rates (of the rule described below) between 20 and 50%. We found that a standard deviation of 0.05 gave good results.

2. Run the model with the proposed candidate. The rule for accepting or rejecting the candidate has two components, namely:

(i). Calculate the ratio of probabilities β, which cancels out the need for estimating $p(D)$:

$$\beta = \frac{p(\theta'|D)}{p(\theta_t|D)} = \frac{p(D|\theta')p(\theta')}{p(D|\theta_t)p(\theta_t)} \qquad [6]$$

(ii). Generate a uniform random variable u ($0 \le u \le 1$). The new candidate θ' is accepted and becomes θ_{t+1} if $u \le \beta$. If $\beta \ge 1$, the proposal is always accepted.

The acceptance criterion, based on the selection of a random variable, thus enables the acceptance of marginal θ_i with probability lower than their predecessor in the chain. This procedure contrasts with many optimisation approaches by allowing downhill steps. The ratio of probabilities, β, also implies that the number of data points used in the calibration has no weight on the selection of a parameter vector (the use of 5 LAI data points instead of 100 has no influence). The weight is given by the data and parameters' uncertainty.

Because the posterior distribution cannot be described analytically, the results are presented in the form of marginal distributions using descriptive statistics. As suggested by Van Oijen et al. (2005), in addition to means and standard deviations, we present the maximum *a posteriori* (MAP) estimate of θ, considered as the single "best" parameter value estimated from the MCMC sample.

$$\theta_{MAPx} = \arg\max_{\theta} p(\theta \mid D) \qquad [7]$$

Although this should not be interpreted as an optimised parameter vector, this nevertheless provides information as to what vector has the highest probability density given the available data.

4.4 Sensitivity analysis

The sensitivity of a given model output with respect to a parameter (and vice versa) has also been estimated from partial correlations calculated between the 25 000 parameter and output vectors. This resulted in a 14x28 partial correlation matrix.

5 Results and discussion

A 25 000 vectors sample was generated from the posterior distribution using the MCMC sampling approach. Figure 4 shows an example of MCMC trace plot and the resulting marginal posterior distribution for the fertility rating (*FR*) parameter.

Figure 4

Summary statistics to the marginal distributions of parameters are presented in Table 3, which include the mean and standard deviation and the vector of highest *a posteriori* probability density (θ_{MAP}). Figure 5 shows the mean model outputs from the 25,000 estimates, the 3-PG outputs from θ_{MAP} (best fit) and the datasets used in the likelihood.

Table 3

Figure 5

Partial correlations between parameters and outputs are presented in Figure 6. These are illustrated under the form of a colour fingerprint between the 14 calibrated parameters and the 28 model outputs. High negative correlations are shown as dark blue and high positive correlations, as dark red. Light regions indicate weak or no correlation.

Figure 6

In Table 3, one can observe the close similarity between the θ_{MAP} vector and the posterior mean $\overline{\theta(i)}$, suggesting that both vectors converge towards a single solution (a local maximum within the full posterior distribution). Corresponding model outputs are shown in Figure 5. Outputs from θ_{MAP} (best fit) and $\overline{\theta(i)}$ (posterior mean) also lie closely to data error bounds. Note the smaller error bounds to the posterior in comparison with the data. While above ground, stem and foliage biomass model dynamics closely match those observed on the ground, allocation to roots appears to level towards 25 years into the rotation and decrease thereafter. This appears to be an artefact of the model structure, rather than parameterisation. Additional MCMC analysis was conducted (results not shown here) to explore the influence of the model structure on the model outputs. The data used in the calibration were given here extremely high standard deviations, such that the distributions tended towards uniform. Likewise, large but realistic ranges of parameter values (with uniform distributions) were given. In doing so, the data became uninformative and the observed dynamics in the model outputs resulted predominantly from the model structure therefore representing "a typical behaviour" and dynamic of the model. In average, the model will tend to produce certain results, unless specific parameterisation is provided. The results showed that in average, 3-PG simulates above-ground growth in an increasing, near linear fashion; LAI follows an exponential increase along the rotation without tail off; and root allocation increases early in the rotation but decreases thereafter (in a similar dynamic as that observed in Figure 5). This suggests that comparatively to above ground biomass and LAI, whose dynamics are sensitive to parameterisation, root biomass is predominantly determined by the model structure. In the Bayesian calibration conducted here, even when data with small uncertainties are used, the underlying influence of the model structure is evident.

Careful examination of Figure 6 also provides strong insights into the multivariate interactions imbedded in the model. For instance, one can observe consistent correlation throughout the rotation between parameters and specific outputs. The optimum temperature for growth, T_{opt} is consistently negatively correlated with all model outputs considered. As T_{opt} increases, productivity is reduced. Most probable

T_{opt} values (θ_{MAP} and $\overline{\theta(i)}$ ≈ 20° C) are reasonable. The species is endemic to elevated altitude Mediterranean regions where hot days are four times more frequent than in Lowland Britain (Brown 1960, Kerr 2000). However, the stands in Thetford seldom grow under optimal temperature where annually, the average temperature is approximately 10° C. Similarly, as the maximum canopy quantum efficiency increases (α_{Cx}), a consistent increase in all biomass outputs is observed. An expected result, as the net primary production is proportional to the product of the maximum canopy quantum efficiency (α_{Cx}), the P_n / P_g ratio (Y), light interception and environmental constraints. Other consistent correlations are found between specific leaf area (σ_1), litterfall rate (γ_{F1}), the ratio of foliage to stem partitioning at maturity (p_{20}) and LAI; between the fertility rating (FR) and above ground components (biomass and LAI); or root turnover (γ_R) and root biomass. As for decreasing or increasing correlations with outputs throughout the rotation, these can provide indications as to where the influence of a parameter is most significant. With Bayesian calibration, the inverse is also true: data collected at specific moments during the rotation may be particularly useful in calibrating and reducing the uncertainty for a given parameter. For instance, maximum stand age (t_x) plays an important role late in the rotation, as it controls productivity reduction as stand ages.

The results presented above serve three purposes. Firstly, they present a first attempt to parameterise 3-PG for Corsican pine stands. While occupying more than 30 thousand hectares of the UK territory (Forestry Commission, 2001), relatively limited information is available on Corsican pines, comparatively to more economically viable species such as Sitka spruce and Scots pine. Thetford forest, one of the largest UK plantations, served as a case study. Model outputs from parameterisation with (i)

θ_{MAP} (parameter vector with highest probability density given available data), and (ii) the mean from the marginal distributions were presented. Secondly, we illustrated the ability of Bayesian calibration as a framework to integrate remote sensing datasets, often the only source of data available at the spatial and temporal scales required, into ecological modelling. This approach enables uncertainty analysis despite the fact that limited data (and often of poor quality), is available. With Bayesian calibration, given relatively diffuse priors (e.g. uniform distributions), the posteriors will be at first strongly influenced by the data. This influence however decreases as new data come in and as the uncertainty in the prior decreases. Thirdly, despite the fact that the probability density of a scalar model output or parameter is nearly nil, process based models used in forestry are commonly parameterised by adjusting the value of selected parameters for the model output to fit the data time series, without any indication of parameter and output uncertainties. The parameterisation of 3-PG for novel species is unfortunately no exception (e.g. White *et al.* 2000, Sands and Landsberg 2002, Sands 2004, Stape *et al.* 2004 and Almeida *et al.* 2004). The results presented here have shown that given ever increasing computing power and speed, uncertainty quantification and model parameterisation can be achieved with relative ease using Bayesian calibration.

6 Conclusion

While both optimisation and Bayesian approaches address the need to test whether a model can predict available data or not, in optimisation, parameter values are adjusted such that the model yields outputs closest to the data. This precludes the integration of uncertain datasets, ancillary or remotely sensed, which can provide information on variables not currently or commonly compiled. Additionally, approaches such as the maximum-likelihood do not enable the full exploration of the parameter landscape. The resulting parameter vector may therefore only be from a local maximum. Conversely, Bayesian calibration advocates the quantification of uncertainties to parameters, thereby yielding uncertainties in model outputs, over the derivation of an optimised set of parameter based on a goodness-of-fit approach (e.g. the maximum-likelihood approach). By doing so, Bayesian calibration provides a means to conduct truly integrative work for quantifying model output and parameter uncertainty, while considering all the existing information, including that enclosed in the model itself.

Acknowledgements

The authors would like to thank Maurizio Mencuccini (University of Edinburgh), David Cameron (CEH Edinburgh), Richard Waring (Oregon State University), and Peter Savill (University of Oxford) for sharing data and advices. Thanks are due to the British Atmospheric Data Centre and the Forestry Commission for providing access to databases, to the Environment Agency for making available the LiDAR data, and to all those involved in the Thetford fieldwork campaigns in 1989 and 2000. The E-SAR data were acquired during the SHAC 2000 campaign by Natural Environmental Research Council and the British National Space Centre.

References

Almeida A.C., Landsberg J.J., Sands P.J. (2004) Parameterisation of 3-PG model for fast-growing Eucalyptus grandis plantations. *Forest Ecology and Management* 193:179-195

Baker J.R. (1992) The UK element of the Maestro-1 SAR campaign. *International Journal of Remote Sensing* 13:1593-1608

Battaglia M., Sands P.J. (1998) Process-based forest productivity models and their application in forest management. *Forest Ecology and Management* 102:13-32

Baulies, X. and Pons, X. (1995). Approach to forestry inventory and mapping by means of multispectral airborne data. International Journal of Remote Sensing, 16:61-80.

Beadle C.L., Jarvis P.G., Talbot H., Neilson R.E. (1985a) Stomatal Conductance and Photosynthesis in a Mature Scots Pine Forest .2. Dependence on Environmental Variables of Single Shoots. *Journal of Applied Ecology* 22:573-586

Beadle C.L., Neilson R.E., Talbot H., Jarvis P.G. (1985b) Stomatal Conductance and Photosynthesis in a Mature Scots Pine Forest .1. Diurnal, Seasonal and Spatial Variation in Shoots. *Journal of Applied Ecology* 22:557-571

Beadle C.L., Talbot H., Jarvis P.G. (1982) Canopy Structure and Leaf-Area Index in a Mature Scots Pine Forest. *Forestry* 55:105-123

Beadle C.L., Talbot H., Neilson R.E., Jarvis PG (1985c) Stomatal Conductance and Photosynthesis in a Mature Scots Pine Forest .3. Variation in Canopy

Conductance and Canopy Photosynthesis. *Journal of Applied Ecology* 22:587-595

Brown, J.M.B. (1960). The Corsican pine in its native island, Part 2. *Empire Forestry Review* 39: 422-436.

Coops N.C., Waring R.H. (2001) The use of multiscale remote sensing imagery to derive regional estimates of forest growth capacity using 3-PGS. *Remote Sensing of Environment* 75 (3): 324-334

Coops N.C., Waring R.H., Landsberg J.J. (2001) Estimation of potential forest productivity across the Oregon transect using satellite data and monthly weather records. *International Journal of Remote Sensing* 22:3797-3812

Corbett W.M. (1973) Breckland forest soils: special survey no.7, Rothamsted Experimental Station, Harpenden, Herts

Cousens J.E. (1988) Report of a 12-Year Study of Litter Fall and Productivity in a Stand of Mature Scots Pine. *Forestry* 61:255-266

Cramer W., Field C.B. (eds) (1999) The Potsdam NPP model intercomparison, *Global Change Biology Vol 5*. Blackwell Science, Oxford.

Edwards P.N., Christie J.M .(1981) Yield models for forest management, *Forestry Commission booklet ; no. 48* HMSO, London, 274 p.

Esprey L.J., Sands P.J., Smith C.W. (2004) Understanding 3-PG using a sensitivity analysis. *Forest Ecology and Management* 193:235-250

Ewel K.C., Gholz H.L. (1991) A Simulation-Model of the Role of Belowground Dynamics in a Florida Pine Plantation. Forest Science 37:397-438

Flower-Ellis J.G.K., Olsson L. (1993) Estimation of volume, total and projected area of Scots pine needles from their regression on lenght. *Studia Forestalia Suecica* 190:1-19

Forestry Commission (2001) National inventory of woodlands and trees. Report No. http://www.forestry.gov.uk/forestry/HCOU-54PG9U, Forest Research, Forestry Commission, Edinburgh

Gash J.H.C., Shuttleworth W.J., Lloyd C.R., Andre J.C., Goutorbe J.P., Gelpe J. (1989) Micrometeorological Measurements in Les-Landes Forest During Hapex-Mobilhy. *Agricultural and Forest Meteorology* 46:131-147

Gertner G.Z., Fang S.F., Skovsgaard J.P. (1999) A Bayesian approach for estimating the parameters of a forest process model based on long-term growth data. *Ecological Modelling* 119:249-265

Ghazoul J., McAllister M. (2003) Communicating complexity and uncertainty in decision making contexts: Bayesian approaches to forest research. *International Forestry Review* 5:9-19

Gill R.A., Jackson R.B. (2000) Global patterns of root turnover for terrestrial ecosystems. *New Phytologist* 147:13-31

Granier A., Biron P., Breda N., Pontailler J.Y., Saugier B. (1996) Transpiration of trees and forest stands: Short and longterm monitoring using sapflow methods. *Global Change Biology* 2:265-274

Green E.J., MacFarlane D.W., Valentine H.T. (2000) Bayesian synthesis for quantifying uncertainty in predictions from process models. *Tree Physiology* 20:415-419

Green E.J., MacFarlane D.W., Valentine H.T., Strawderman W.E. (1999) Assessing uncertainty in a stand growth model by Bayesian synthesis. *Forest Science* 45:528-538

Hamilton G.J. (1975) Forest mensuration handbook, *Forestry Commission booklet no. 39* HMSO, London, 274 p.

Hyyppä J., Hyyppä H., Inkinen M., Schardt M., Ziegler M. (2000). Forest inventory based on laser scanning and aerial photography. *Laser Radar Technology and Applications*, V:106-118.

Hyyppä, J., Kelle, O., Lehikoinen, M., Inkinen, M. A (2001). segmentation-based method to retrieve stem volume estimates from 3-D tree height models produced by laser scanners. *IEEE Transactions on Geoscience and Remote Sensing*, 39 (5): 969-975.

Jansen M.J.W. (1999) Data use and Bayesian statistics for model calibration. In: Stein A., Penning de Vries F.W.T. (eds) *Data and models in action*. Kluwer, Dordrecht, p 69-80

Kelliher F.M., Leuning R., Raupach M.R., Schulze E.D. (1995) Maximum Conductances for Evaporation from Global Vegetation Types. *Agricultural and Forest Meteorology* 73:1-16

Kelliher F.M., Leuning R., Schulze E.D. (1993) Evaporation and Canopy Characteristics of Coniferous Forests and Grasslands. *Oecologia* 95:153-163

Kerr, G. (2000). Natural regeneration of Corsican pine (Pinus nigra subsp laricio) in Great Britain. *Forestry* 73(5): 479-488.

Landsberg J.J., Waring R.H. (1997) A generalised model of forest productivity using simplified concepts of radiation-use efficiency, carbon balance and partitioning. *Forest Ecology and Management* 95:209-228

Law B.E., Waring R.H., Anthoni P.M., Aber J.D. (2000) Measurements of gross and net ecosystem productivity and water vapour exchange of a *Pinus ponderosa* ecosystem, and an evaluation of two generalized models. *Global Change Biology* 6:155-168

Levy P.E., Hale S.E., Nicoll B.C. (2004) Biomass expansion factors and root : shoot ratios for coniferous tree species in Great Britain. *Forestry* 77:421-430

Luckman A., Baker J., Kuplich T.M., Yanasse C.D.F., Frery A.C. (1997) A study of the relationship between radar backscatter and regenerating tropical forest biomass for spaceborne SAR instruments. *Remote Sensing of Environment* 60:1-13

Mencuccini M., Grace J. (1996) Hydraulic conductance, light interception and needle nutrient concentration in Scots pine stands and their relations with net primary productivity. *Tree Physiology* 16:459-468

New M., Hulme M. and Jones P. (2000) Representing twentieth-centurey space-time climate variability. Part II: Development of 1901-96 monthly grids of terrestrial surface climate. *Journal of Climate* 13(13):2217-2238 http://www.cru.uea.ac.uk/~markn/cru05/cru05_intro.html

Ovington J.D. (1957) Dry-matter production by *Pinus sylvestris* L. *Annals of Botany* XXI:288-314

Roberts J.M. (1976) A study of root distribution and growth in a Pinus sylvestris L. (scots pine) plantation in East Anglia. *Plant and Soil* 44:607-621

Running S.W., Coughlan J.C. (1988) A general model of forest ecosystem processes for regional applications I. Hydrological balance canopy gas exchange and primary production processes. *Ecological Modelling* 42:125-154

Rowland C.S, Patenaude G., Balzter H., Dawson T.P., Hill R.A., Luckman A., Milne R., Skinner L. (2003) Forest carbon estimation: a comparison of techniques, annual meeting of the Remote Sensing and Photogrammetry Society.

Sands P.J. (2004) Adaptation of 3-PG to novel species : guidelines for data collection and parameter assignment. *Technical Report. No. 141*, CSIRO, CRC Sustainable Production Forestry, Hobart

Sands P.J., Landsberg J.J. (2002) Parameterisation of 3-PG for plantation grown Eucalyptus globulus. *Forest Ecology and Management* 163:273-292

Skinner L., Luckman A. (2000) Thetford forest ground data collection campaign in support of the SHAC SAR aquisition, June 2000, University of Wales Swansea, Swansea, Unpublished report 34p.

Stape J.L., Ryan M.G., Binkley D. (2004) Testing the utility of the 3-PG model for growth of Eucalyptus grandis X urophylla with natural and manipulated supplies of water and nutrients. Forest Ecology and Management 193:219-234

Stenberg P., Kuuluvainen T., Kellomaki S., Grace J.C., Jokela E.C., Gholz H.L. (1994) Crown structure, light interception and productivity of pine trees and stands. *Ecological Bulletins* 43:20-34

Stewart J.B. (1988) Modeling Surface Conductance of Pine Forest. *Agricultural and Forest Meteorology* 43:19-35

Vanclay J.K. (1989) A growth model for North Queensland rainforests. *Forest Ecology and Management* 27:245-271

van Hees A.F.M., Bartelink H.H. (1993) Needle Area Relationships of Scots Pine in the Netherlands. *Forest Ecology and Management* 58:19-31

Van Oijen M., Rougier J., Smith R. (2005) Bayesian calibration of process-based models: bridging the gap between models and data. *Tree Physiology* 25 (7): 915-927

Wang K.Y., Kellomaki S., Zha T.S., Peltola H. (2004) Component carbon fluxes and their contribution to ecosystem carbon exchange in a pine forest: an assessment based on eddy covariance measurements and an integrated model. . 24:19-34

Wang Y.P., Jarvis P.G. (1990) Description and Validation of an Array Model - Maestro. *Agricultural and Forest Meteorology* 51:257-280

Waring R.H. (2000) A process model analysis of environmental limitations on the growth of Sitka spruce plantations in Great Britain. *Forestry* 73:65-79

Waring R.H., Running S.W. (1998) *Forest ecosystems : analysis at multiple scales*, 2nd Ed. Academic Press, London 270 p.

White J.D., Coops N.C., Scott N.A. (2000) Estimates of New Zeland forest and scrub biomass from the 3-PG model. *Ecological Modelling* 131:175-190

Figure 1

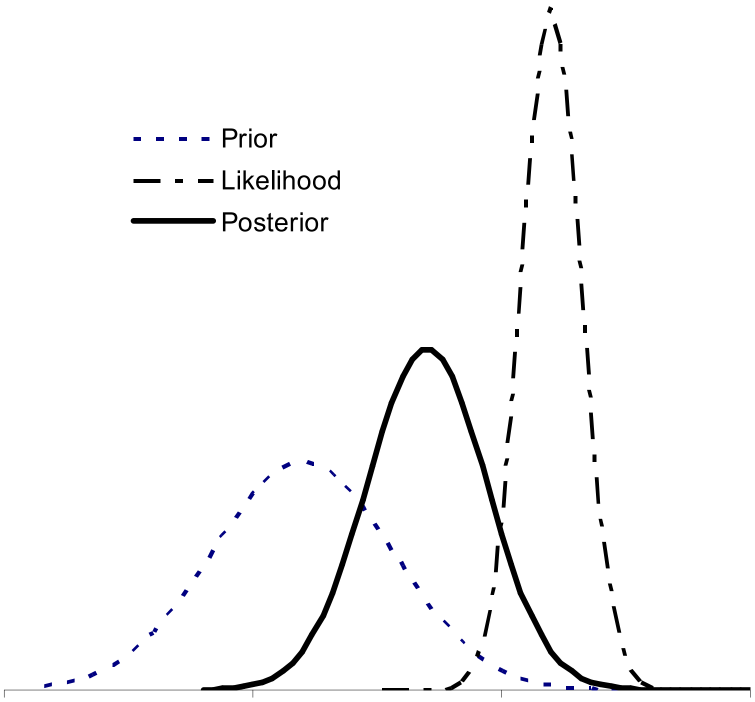

Figure 2

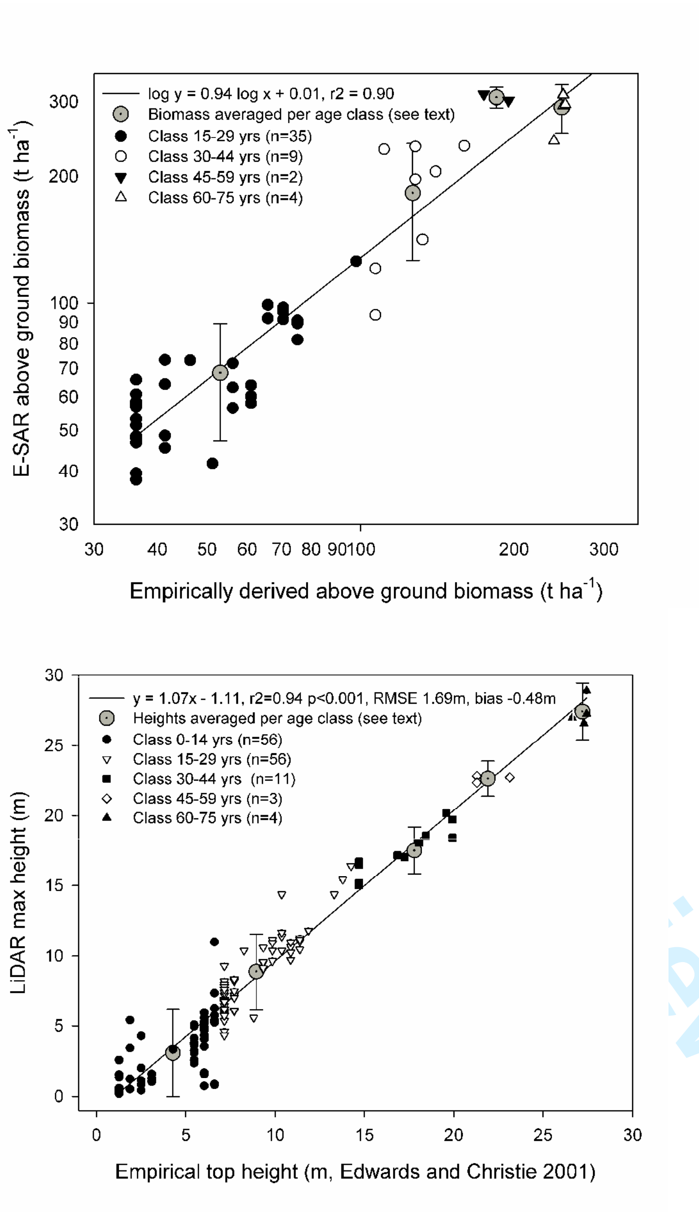
log y = 0.94 log x + 0.01, r2 = 0.90
Biomass averaged per age class (see text)
Class 15-29 yrs (n=35)
Class 30-44 yrs (n=9)
Class 45-59 yrs (n=2)
Class 60-75 yrs (n=4)
E-SAR above ground biomass (t ha^{-1})
Empirically derived above ground biomass (t ha^{-1})
30
40
50
60
70
80
90
100
200
300
30
40
50
60
70
80
90100
200
300
y = 1.07x - 1.11, r2=0.94 p<0.001, RMSE 1.69m, bias -0.48m
Heights averaged per age class (see text)
Class 0-14 yrs (n=56)
Class 15-29 yrs (n=56)
Class 30-44 yrs (n=11)
Class 45-59 yrs (n=3)
Class 60-75 yrs (n=4)
LiDAR max height (m)
Empirical top height (m, Edwards and Christie 2001)
0
5
10
15
20
25
30
0
5
10
15
20
25
30

Figure 3

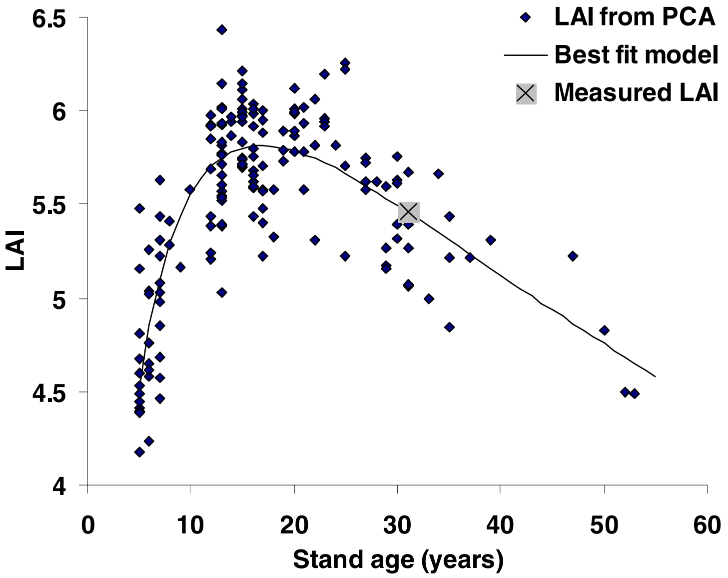
6.5
6
5.5
5
4.5
4
LAI
0
10
20
30
40
50
60
Stand age (years)
LAI from PCA
Best fit model
Measured LAI

Figure 4

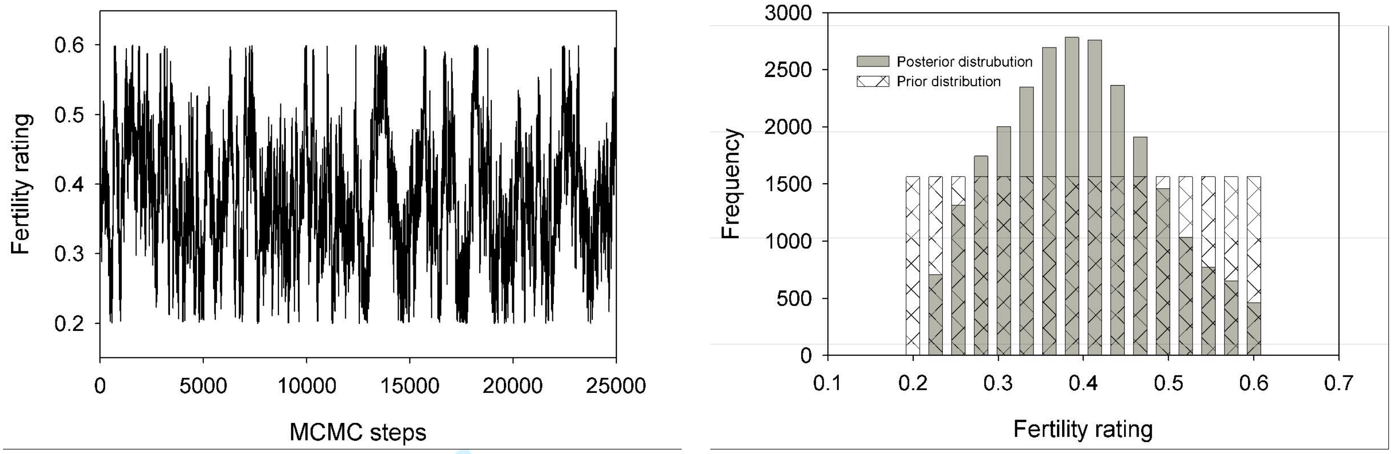
Fertility rating
0.6
0.5
0.4
0.3
0.2
0
5000
10000
15000
20000
25000
MCMC steps
Frequency
3000
2500
2000
1500
1000
500
0
Posterior distrubution
Prior distribution
0.1
0.2
0.3
0.4
0.5
0.6
0.7
Fertility rating

Figure 5

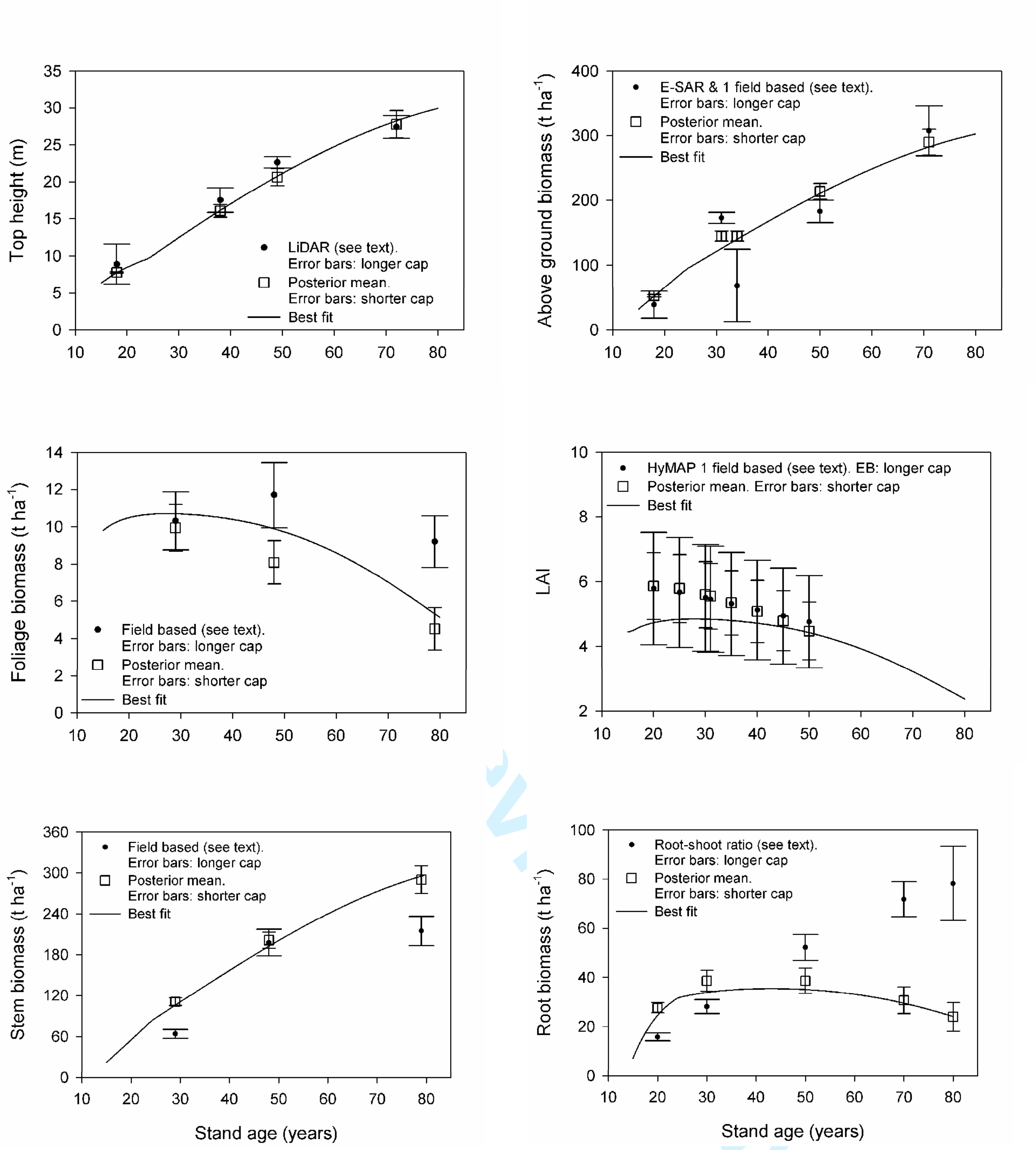
Top height (m)
35
30
25
20
15
10
5
0
10 20 30 40 50 60 70 80
● LiDAR (see text).
Error bars: longer cap
□ Posterior mean.
Error bars: shorter cap
Best fit
Above ground biomass (t ha^{-1})
400
300
200
100
0
10 20 30 40 50 60 70 80
● E-SAR & 1 field based (see text).
Error bars: longer cap
□ Posterior mean.
Error bars: shorter cap
Best fit
Foliage biomass (t ha^{-1})
14
12
10
8
6
4
2
0
10 20 30 40 50 60 70 80
● Field based (see text).
Error bars: longer cap
□ Posterior mean.
Error bars: shorter cap
Best fit
LAI
10
8
6
4
2
10 20 30 40 50 60 70 80
● HyMAP 1 field based (see text). EB: longer cap
□ Posterior mean. Error bars: shorter cap
Best fit
Stem biomass (t ha^{-1})
360
300
240
180
120
60
0
10 20 30 40 50 60 70 80
● Field based (see text).
Error bars: longer cap
□ Posterior mean.
Error bars: shorter cap
Best fit
Stand age (years)
Root biomass (t ha^{-1})
100
80
60
40
20
0
10 20 30 40 50 60 70 80
● Root-shoot ratio (see text).
Error bars: longer cap
□ Posterior mean.
Error bars: shorter cap
Best fit
Stand age (years)

Figure 6:

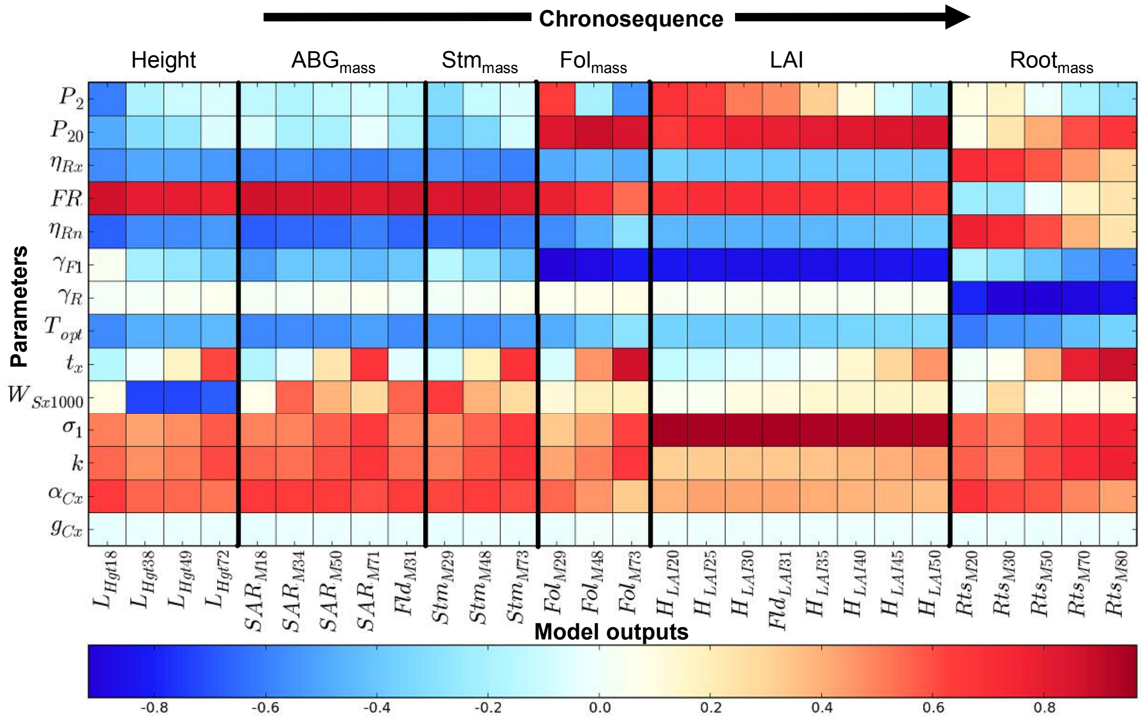

GREY VERSION (if colour printer unavailable)

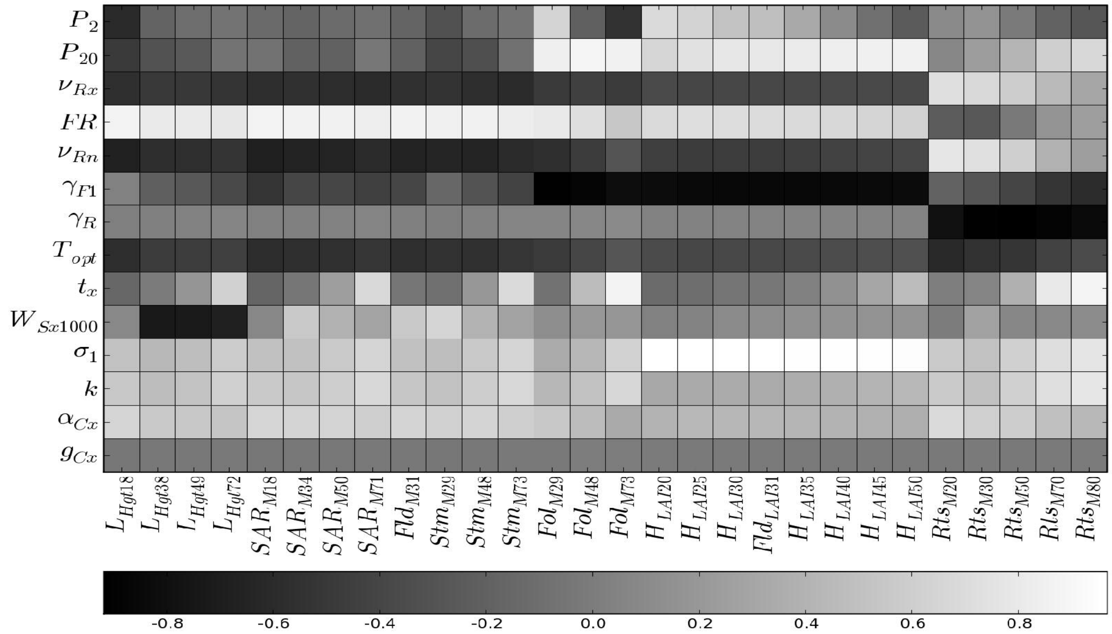

Table 1:

Monthly Climate data	Mean Tmax[a.] (°C)	Mean Tmin [a.] (°C)	Rain [b.] (mm)	Solar rad [b.] (MJ $m^{-2}d^{-1}$)	Frost days [a.] (days)
January	6.47	1.08	55.0	2.52	10.7
Feb	7.29	0.97	42.4	4.53	11.2
March	10.18	2.13	51.9	8.26	7.9
April	13.13	3.95	48.0	13.10	3.3
may	16.86	6.70	55.0	16.58	0.8
June	20.08	9.73	55.0	18.43	0.0
July	22.31	11.83	54.0	16.64	0.0
Aug	22.15	11.58	58.0	14.42	0.0
Sep	19.17	9.64	61.1	10.00	0.0
Oct	14.99	6.66	61.1	5.80	1.5
Nov	10.07	3.51	69.0	2.86	5.7
Dec	12.61	2.04	61.1	1.96	9.1

Table 2

3-PG symbol: Description (units)	**S Class**[a]	**Prescribed Parameter Values**	**Calibrated Parameters: ranges of values in the prior**		**Data Class**[b]	**Source/Comment**
	.		θ_{min}	θ_{max}		
a_S: Constant in stem mass *v* diam. relationship	M	0.02	-	-	CP-T	Baker 1992, Baker *et al.* 1994, Edwards and Christie 1981.
c_θ: Moisture ratio deficit which gives $f_\theta = 0.5$	H	0.7	-	-	D	Default for sandy soils
f_{N0}: Value of f_N when $FR = 0$	M	0.6	-	-	D	
FR: Fertility rating	?	-	0.2	0.6	CP-T	Soil Fertility (Corbett 1973, Roberts et al. 1982)
g_B: Canopy boundary layer conductance (m s^{-1})	L	0.2	-	-	D	
g_{Cx}: Maximum canopy conductance (m s^{-1})	H	-	0.015	0.03	P-L	Kelliher *et al.* 1995
i_{Rx}: Maximum fraction of rainfall intercepted by canopy	M	0.15	-	-	D	
k: Extinction coefficient for PAR absorption by canopy	M	-	0.4	0.7	P-L	Stenberg *et al.* 1994, Mencuccini and Grace 1996
k_F: Number of days production lost for each frost day	L	1	-	-	D	
L_{Cx}: Canopy LAI for maximum canopy conductance (m^2 m^{-2})	L	3.33	-	-	P-L	Kelliher *et al.* 1995, Mencuccini and Grace, 1996
L_{ix}: LAI for maximum rainfall interception (m^2 m^{-2})	L	0	-	-	D	
m_0: Value of m when $FR = 0$	?	0	-	-	D	
m_F: Fraction of mean foliage biomass per dying tree	L	0	-	-	D	
m_R: Fraction of mean root biomass per dying tree	L	0.2	-	-	P-L	Empirical data (Edwards and Christie 1981,Ovington 1957)
m_S: Fractions of mean stem biomass per dying tree	L	0.2	-	-	CP-L	Empirical data (Edwards and Christie 1981)
n_{age}: Power of relative age in f_{age}	L	4	-	-	D	
n_N: Power in self thinning law	L	1.5	-	-	P-L	Theoretical scaling laws & observation
n_{fN}: Power of (1-FR) in f_N	L	1	-	-	D	
n_S: Power in stem mass *v* diam. Relationship	H	2.88	-	-	CP-T	Baker 1992, Baker *et al.* (1994), Edwards and Christie 1981

n_θ: Power of moisture ratio deficit in f_θ	L	9	-	-	D	Default for sandy soils
p_2: Ratio of foliage:stem partitioning at $B = 2$ (cm)	H	-	0.5	1	P-L	Gower *et al*. 1994
p_{20}: Ratio of foliage:stem partitioning at $B = 20$ (cm)	H	-	0.1	0.5	P-L	Gower *et al*. 1994
p_{BB0}: Branch and bark fraction at stand age 0	L	0.5	-	-	P-L	Default 3-PG values for P.radiata
p_{BB1}: Branch and bark fraction for mature aged stands	L	0.1	-	-	P-L	Default 3-PG values for P.radiata
r_{age}: Relative age to give $f_{age} = 0.5$	L	0.95	-	-	D	
t_{BB}: Age at which $p_{BB} = ½(p_{BB0} + p_{BB1})$	L	5	-	-	P-L	Default 3-PG values for P.radiata
t_c: Age at full canopy cover (yr)	M	0	-	-	P-L	
T_{max}: Maximum temperature for growth (ºC)	L	35	-	-	P-L	
T_{min}: Minimum temperature for growth (ºC)	L	0	-	-	D	
T_{opt}: Optimum temperature for growth (ºC)	M	-	18	22	P-L	Waring and Running, 1998
t_x: Maximum stand age used to compute relative age (year)	L	-	60	100	D	10% of age at maximum height (Waring, pers. Comm.)
$t_{\gamma F}$: Age at which litterfall rate has median value (month)	L	36	-	-	D	
t_σ: Age at which specific leaf area = $½(\sigma_0+\sigma_1)$ (yr)	L	2.5	-	-	D	
W_{Sx1000}: Maximum stem mass per tree at 1000 trees/ha		-	160	400	CP-L	live stem numbers time-series: Edwards and Christie (1981)
Y: Ratio NPP/GPP	H	0.47	-	-	P-L	Waring & Running (1998)
α_{Cx}: Maximum canopy quantum efficiency (mol mol^{-1})	H	-	0.045	0.065	P-L	Range for temperate species in 3-PG (e.g. Stenberg *et al*. 1994, Law et al. 2000, Waring 2000, Waring et al. 2002, Wang *et al*. 2004)
γ_{F0}: Litterfall rate at $t = 0$ (month^{-1})	L	0.001	-	-	D	
γ_{F1}: Litterfall rate for mature stands (month^{-1})	H	-	0.025	0.035	P-T	Beadle *et al*. 1982, Cousens (1988)
γ_R: Average monthly root turnover rate (month^{-1})	L	-	0.006	0.015	P-L	Gill & Jackson (2000)
η_{Rn}: Minimum fraction of NPP to roots	M	-	0.20	0.50	P-T	Ovington (1957), Levy *et al*. (2004)
η_{Rx}: Maximum fraction of NPP to roots	M	-	0.50	0.80	P-T	Ovington 1957, Levy *et al*. (2004)
σ_0: Specific leaf area at stand age 0 (m^2 kg^{-1})	L	5			P-L	VanHees & Bartelink (1993)
σ_1: Specific leaf area for mature aged stands (m^2 kg^{-1})	H	-	4	8	P-L	VanHees & Bartelink (1993)
ρ_1: Basic density	H	0.43	-	-	CP-L	Hamilton (1975)

Table 3:

$\theta(i)$	$\overline{\theta(i)}$	***SD***	θ_{MAPx}
FR	0.380	0.090	0.391
g_{Cx}	0.023	0.004	0.023
K	0.539	0.087	0.439
p_2	0.694	0.133	0.502
p_{20}	0.441	0.045	0.497
T_{opt}	20.893	0.911	20.42
t_x	90.656	6.978	95.86
w_{Sx1000}	182.826	17.504	165.0
α_{Cx}	0.047	0.002	0.046
γ_{F1}	0.028	0.003	0.026
γ_R	0.013	0.002	0.013
η_{Rn}	0.237	0.028	0.221
η_{Rx}	0.580	0.067	0.557
σ_1	5.711	1.029	4.539